



RESEARCH ARTICLE

A novel pulsar-based template-independent navigation method

Zhize Li, Wei Zheng,* and Yusong Wang

College of Aerospace Science and Engineering, National University of Defense Technology, Changsha, China.

*Corresponding author. E-mail: zhengwei@nudt.edu.cn

Received: 15 December 2021; **Accepted:** 27 May 2022; **First published online:** 17 August 2022

Keywords: template-independent; pulsar-based navigation; orbital transition matrix; multi-segment observations

Abstract

Because of the high photon flux, the Crab nebula pulsar is widely used as the observation target for X-ray pulsar-based navigation. The built profile of the Crab pulsar will change over time, however, which means that the pre-calibrated template cannot be used for the long term. In this paper, a novel pulsar-based template-independent navigation method is proposed. The detected phase propagation model is given as a term of position of the vehicle, taking the orbital motion into account. A different method of time-of-arrival process between the recovered profiles is introduced. With the aid of orbital transition matrix, a measurement model is derived to be a term of velocity error of the vehicle varying with time. The state errors of the vehicle are transformed into velocity errors by performing multi-segment observations to achieve the navigation system observability. The navigation equations of the system are then established and can be solved directly. Some simulations are performed to verify the method and suggest that the proposed method is feasible, effective and easy to implement. The precise orbit information of the vehicle can be determined. The state estimation accuracy is basically consistent with the traditional filtering algorithms, and the computational cost is still very low.

1. Introduction

X-ray pulsar-based navigation (Chester and Butman, 1981) is a novel astronomical autonomous navigation method with the following advantages that traditional navigation methods lack. (1) It has a wide range of application with high stability. It is applicable to both near-Earth and deep space (Shuai et al., 2006). (2) The navigation accuracy does not change with the position of the vehicle. This is related to the performance of X-ray sensors (Song et al., 2009), which means that there is still great development potential in the future. (3) Pulsars are like natural beacons with long-term high signal period stability (Lyne and Graham-Smith, 2005) and can provide navigation information along with time reference. (4) To some extent, pulsar-based navigation can provide navigation service without using a filtering algorithm (Li, 2015).

As the X-ray pulsar signal is discontinuous and extremely weak, an onboard sensor needs to observe the target pulsar for a long time to accumulate enough photons. Considering the orbital motion of the vehicle, the varying Doppler effect and the unknown accuracy of information on state make it difficult to solve the navigation measurements (Emadzadeh, 2009; Winternitz et al., 2015). To deal with this problem, the method of dynamic signal processing was proposed (Wang and Zheng, 2016a, 2016b). The modified phase propagation model is given, and the predicted orbit information of the vehicle used can be obtained by propagating the initial state with the aid of an orbital dynamic model. The pulse TOA (time-of-arrival) can then be acquired through epoch folding (Emadzadeh and Speyer, 2011a, 2011b) or maximum likelihood estimation (Golshan and Sheikh, 2008; Li and Ke, 2011).

For the current principle of pulsar-based navigation (Hanson, 1996; Huang et al., 2013; Xue et al., 2021), the pulse TOA is calculated by comparing the modified observation profile with the pulsar template, and then the required navigation measurements can be obtained. With the aid of filtering algorithms, the state estimation of the vehicle can be achieved by processing the measurements in one or more orientations (Zhang, 2018b). Limited by the effective area of the current onboard X-ray sensor and considering the signal-to-noise ratio requirement of the detected signal, only pulsars with high photon flux are suitable as observation targets. On this account, the Crab nebula pulsar becomes the best target for observation. However, the theoretical framework of existing methods is established on the assumption that the template of the pulsar is accurate and stable over time. But for the Crab pulsar, the short-term frequency is unstable and there is also the presence of more frequent glitches. The built profile of the Crab pulsar will change over time, which means that the timing model and the corresponding parameters of frequency must be updated frequently, and the pre-calibrated template cannot be used in the long term (Zhang, 2018a). It is also quite difficult and time-consuming to recover a high precision template of the Crab pulsar in orbit (Wang, 2016). If the utilised template includes a phase error, it will directly affect the estimation accuracy of pulse TOA and reduce the performance of the navigation system (Sun et al., 2014). Therefore, research into the template-independent method is of great practical significance.

In this paper, to answer the situations where there is no standard template or the built template is not accurate, a template-independent navigation method for multi-segment observation of a single pulsar is proposed. Taking the motion of the vehicle into account, the detected signal model of the X-ray pulsar is given as a term of vehicle position varying with time. The measurement model as a term of velocity error of the vehicle is derived with the aid of the orbital transition matrix. In this part, a different method of TOA process is used to obtain the navigation measurements without considering the pulsar template, which denotes a distort phase difference between the modified observation profile and the directly recovered one. Given that the state of the vehicle at later epochs can be predicted by propagation of the initial state, to achieve the navigation system observability, the state errors of the vehicle can be transformed completely into the velocity errors by performing multi-segment observations. The initial state is set as variables and substituted into the set of the deduced measurement model to calculate the orbital transition coefficient matrix. The navigation equations are then established. Orbit or navigation information can be achieved finally by solving the constructed equations. The simulation results demonstrate that the estimated state errors are basically consistent with the traditional filtering algorithms.

This paper is organised into five sections. After the introduction, the measurement model as a term of velocity error of the vehicle is derived in Section 2. The proposed template-independent pulsar-based navigation method is described in Section 3. Some simulations are performed in Section 4 to demonstrate the comprehensive performance of the presented method. Conclusions are drawn in Section 5.

2. Modified measurement model without considering the pulsar template

This paper studies a novel method of pulsar-based navigation, where the point is to avoid dependency on the template of the Crab pulsar. Schematics of three pulse profiles commonly used in dynamic signal processing are shown in Figure 1. The pulsar template is the basic input to the existing methods for calculating the pulse TOA, which usually needs two or three days of accumulated observation data to build. The modified observation profile in this paper is the pulse profile recovered after period search (Zhou et al., 2013), the Doppler effects from the motion of the vehicle are basically eliminated. The observation profile is that directly recovered with the prior information of pulsar frequency.

For the existing theoretical framework of pulsar-based navigation, the pulse TOA can be calculated by the phase difference between the modified observation profile and the pulsar template. The general measurement model is

$$\Delta\text{TOA}_1 = \frac{1}{c} \mathbf{n} \Delta \mathbf{r} \quad (1)$$

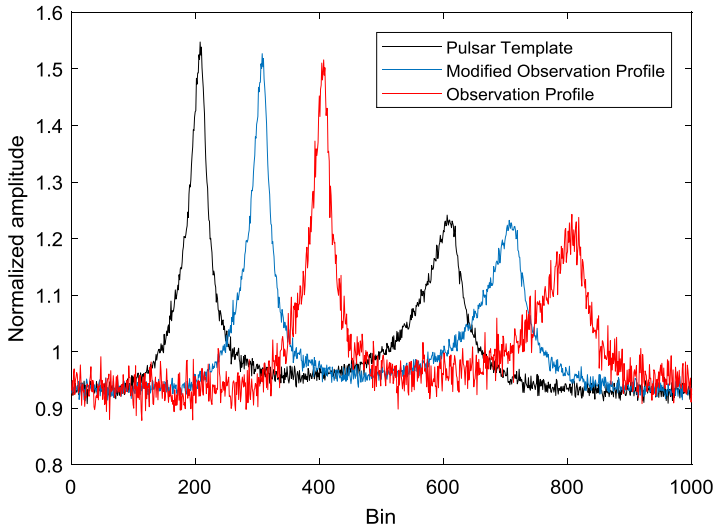


Figure 1. Schematic of observation profiles used in dynamic signal processing.

where \mathbf{n} denotes the direction of the pulsar, c is the speed of light, and $\Delta \mathbf{r}$ usually represents the distance between the investigated vehicle and SSB (solar system barycentre).

For the Crab pulsar, however, the aim here is to find a different method of TOA process without using the template. We can easily find that only the frequency parameters of the pulsar used for building the profile are different between the other two recovered profiles. So, there will remain a distort phase difference. As the recovered profiles are integrated with all pulses during the observation period, this distort phase difference should equal the mean phase propagation error over the entire period, which can be converted to a relative expression of velocity error of the vehicle at a given moment, in theory. This distort phase difference can also be regarded as a difference model between two kinds of phase propagation error based on the pulsar template with the advantage that most system errors can be ignored. There is also no need to consider the problem of ambiguity of whole cycles.

With reference to the beginning of the observation t_0 , the detected phase propagation model at the onboard sensor is (Emadzadeh and Speyer, 2011a)

$$\phi_{\text{det}}(t) = \phi_0 + \int_{t_0}^t f(\tau) d\tau \tag{2}$$

where ϕ_0 is the initial phase at t_0 , $f(t)$ is the observed signal frequency, which can be decomposed into two different components: X-ray source frequency f_s (the spinning frequency of pulsar), and the Doppler frequency shift $f_d(t) = f_s \frac{v(t)}{c}$.

Taking the orbiting motion of the vehicle into account, $\phi_{\text{det}}(t)$ can be written as

$$\phi_{\text{det}}(t) = \phi_0 + f_s(t - t_0) + \frac{f_s}{c} \int_{t_0}^t v(\tau) d\tau \tag{3}$$

where v is the vehicle’s velocity projected on the direction of the pulsar.

Given that the pulsar is far from the solar system, the velocity of the vehicle projected along the direction of the pulsar is

$$v = \mathbf{n} \cdot (\dot{\mathbf{r}} - \dot{\mathbf{D}}) \tag{4}$$

where \mathbf{r} is the position of the vehicle relative to SSB, \mathbf{D} is the position of the pulsar in the same reference system.

Substituting Equation (4) into Equation (3) yields

$$\phi_{\text{det}}(t) = \phi_0 + f_s(t - t_0) + \frac{f_s}{c} \int_{t_0}^t \mathbf{n} \cdot \dot{\mathbf{r}}(\tau) d\tau - \frac{f_s}{c} \int_{t_0}^t \mathbf{n} \cdot \dot{\mathbf{D}}(\tau) d\tau \tag{5}$$

Then, if the proper motion of the pulsar during the observation period can be neglected, that is, $\mathbf{D}(t) \approx \mathbf{D}(t_0)$, the detected phase propagation model can be simplified as (Wang, 2016)

$$\phi_{\text{det}}(t) = \phi_0 + f_s(t - t_0) + \frac{f_s}{c} \mathbf{n} \cdot (\mathbf{r}(t) - \mathbf{r}(t_0)) \tag{6}$$

The true state of the vehicle at an arbitrary epoch t can be expressed as the term of predicted state and propagation error.

$$\begin{cases} \mathbf{r}(t) = \tilde{\mathbf{r}}(t) + \delta\mathbf{r}(t) \\ \mathbf{v}(t) = \tilde{\mathbf{v}}(t) + \delta\mathbf{v}(t) \end{cases} \tag{7}$$

where $\tilde{\mathbf{r}}(\cdot)$ and $\tilde{\mathbf{v}}(\cdot)$ denote the predicted position and velocity, $\delta\mathbf{r}(\cdot)$ and $\delta\mathbf{v}(\cdot)$ denote the corresponding propagation errors.

Substituting Equation (7) into Equation (6) we have

$$\phi_{\text{det}}(t) = \phi_0 + f_s(t - t_0) + \frac{f_s}{c} \mathbf{n} \cdot (\tilde{\mathbf{r}}(t) - \tilde{\mathbf{r}}(t_0)) + \frac{f_s}{c} \mathbf{n} \cdot (\delta\mathbf{r}(t) - \delta\mathbf{r}(t_0)) \tag{8}$$

To subtract $\frac{f_s}{c} \mathbf{n} \cdot (\tilde{\mathbf{r}}(t) - \tilde{\mathbf{r}}(t_0))$, which is called the orbital motion effect term, all the photon TOAs should be transformed to the position of the vehicle at t_0 with the aid of predicted state information. Equation (7) can then be rewritten as

$$\phi_{\text{det}}(t) = \phi_0 + f_s(t - t_0) + \frac{f_s}{c} \mathbf{n} \cdot (\delta\mathbf{r}(t) - \delta\mathbf{r}(t_0)) \tag{9}$$

Assume that the observation period is $T_{\text{obs}} = T - t_0$ and comprising N_p pulsar periods, namely, $T_{\text{obs}} = N_p P$. In the i th bin, the profile function after epoch folding can be represented as (Emadzadeh and Speyer, 2011b)

$$\begin{aligned} \hat{\lambda}(t_i) &= \frac{1}{N_p} \sum_{i=1}^{N_p} \lambda \left(t_i; \phi_0 + \frac{f_s}{c} \mathbf{n} \cdot (\delta\mathbf{r}(iP) - \delta\mathbf{r}(t_0)) \right) + n(t_i) \\ &\approx \lambda(t_i; \phi_0) + \frac{1}{N_p} \sum_{i=1}^{N_p} \lambda \left(\frac{f_s}{c} \mathbf{n} \cdot (\delta\mathbf{r}(iP) - \delta\mathbf{r}(t_0)) \right) \end{aligned} \tag{10}$$

where P denotes the period of the pulsar, $\lambda(\cdot)$ is the photon rate function of the pulsar signal, $\lambda'(\cdot)$ expresses the derivative of $\lambda(\cdot)$ and t_i denotes the middle time of the i th bin. $n(t_i)$ is referred to the epoch folding noise, which is uncorrelated over a long observation time.

Using the orbital transition matrix, $\delta\mathbf{r}(iP)$ can be expressed as a term of $\delta\mathbf{r}(t_0)$ and $\delta\mathbf{v}(t_0)$, i.e.,

$$\delta\mathbf{r}(iP) = \Phi_{rr}(iP, t_0) \delta\mathbf{r}(t_0) + \Phi_{rv}(iP, t_0) \delta\mathbf{v}(t_0) \tag{11}$$

where $\Phi_{rr}(t, t_0)$ and $\Phi_{rv}(t, t_0)$ are the partition matrices of orbital transition matrix (Zhang, 2015), and the concrete expressions can be found in the appendix.

Substituting Equation (11) into Equation (10) yields

$$\hat{\lambda}(t_i) \approx \lambda(t_i; \phi_0) + \lambda'(t_i; \phi_0) \left\{ \begin{aligned} & \frac{f_s}{c} \mathbf{n} \cdot \sum_{i=1}^{N_p} \left[\left(\Phi_{rr} \left(i \frac{T_{obs}}{N_p}, t_0 \right) - \mathbf{I}_{3 \times 3} \right) \frac{1}{N_p} \right] \delta \mathbf{r}(t_0) \\ & + \frac{f_s}{c} \mathbf{n} \cdot \sum_{i=1}^{N_p} \left[\Phi_{rv} \left(i \frac{T_{obs}}{N_p}, t_0 \right) \frac{1}{N_p} \right] \delta \mathbf{v}(t_0) \end{aligned} \right\} \quad (12)$$

The period of the pulsar is much smaller than the whole observation time. It can therefore be considered that $N_p \rightarrow \infty$, then we can obtain

$$\begin{aligned} & \frac{f_s}{c} \mathbf{n} \cdot \sum_{i=1}^{N_p} \left[\left(\Phi_{rr} \left(i \frac{T_{obs}}{N_p}, t_0 \right) - \mathbf{I}_{3 \times 3} \right) \frac{1}{N_p} \right] \delta \mathbf{r}(t_0) \\ & \approx \frac{f_s}{c T_{obs}} \mathbf{n} \cdot \left(\int_{t_0}^T \Phi_{rr}(\tau, t_0) d\tau - T_{obs} \mathbf{I}_{3 \times 3} \right) \delta \mathbf{r}(t_0) \end{aligned} \quad (13)$$

$$\frac{f_s}{c} \mathbf{n} \cdot \sum_{i=1}^{N_p} \left[\Phi_{rv} \left(i \frac{T_{obs}}{N_p}, t_0 \right) \frac{1}{N_p} \right] \delta \mathbf{v}(t_0) \approx \frac{f_s}{c T_{obs}} \mathbf{n} \cdot \left(\int_{t_0}^T \Phi_{rv}(\tau, t_0) d\tau \right) \delta \mathbf{v}(t_0) \quad (14)$$

Make $\Delta\lambda$ represent the propagation effects of initial error.

$$\Delta\lambda = \frac{f_s}{c T_{obs}} \left\{ \begin{aligned} & \mathbf{n} \cdot \left(\int_{t_0}^T \Phi_{rr}(\tau, t_0) d\tau - T_{obs} \mathbf{I}_{3 \times 3} \right) \delta \mathbf{r}(t_0) \\ & + \mathbf{n} \cdot \left(\int_{t_0}^T \Phi_{rv}(\tau, t_0) d\tau \right) \delta \mathbf{v}(t_0) \end{aligned} \right\} \begin{bmatrix} \lambda'(t_1; \phi_0) \\ \lambda'(t_2; \phi_0) \\ \vdots \\ \lambda'(t_{N_b}; \phi_0) \end{bmatrix} \quad (15)$$

The additional phase estimation error caused by $\Delta\lambda$ can be written as

$$\Delta\hat{\phi} = (\mathbf{H}^T \mathbf{H})^{-1} \mathbf{H}^T \Delta\lambda \quad (16)$$

where

$$\mathbf{H} = \lambda'(\phi_0) \quad (17)$$

Substitute $\Delta\lambda$ into Equation (16), then we can derive the expression of additional phase estimation error caused by the propagation effects of initial error.

$$\begin{aligned} \Delta\hat{\phi} &= \frac{f_s}{c T_{obs}} \mathbf{n} \cdot \left(\int_{t_0}^T \Phi_{rr}(\tau, t_0) d\tau - T_{obs} \mathbf{I}_{3 \times 3} \right) \delta \mathbf{r}(t_0) \\ &+ \frac{f_s}{c T_{obs}} \mathbf{n} \cdot \left(\int_{t_0}^T \Phi_{rv}(\tau, t_0) d\tau \right) \delta \mathbf{v}(t_0) \end{aligned} \quad (18)$$

where $\Delta\hat{\phi}$ represents the distort phase difference between the modified observation profile and the directly recovered one.

From simple simulation, the value of the term $\frac{f_s}{c T_{obs}} \mathbf{n} \cdot \left(\int_{t_0}^T \Phi_{rr}(\tau, t_0) d\tau - T_{obs} \mathbf{I}_{3 \times 3} \right) \delta \mathbf{r}(t_0)$ is extremely small and can be neglected in Equation (18). For the vehicle in Earth orbit, for every 10 km increase in the position error, the value only increases by about 1×10^{-5} , which is much lower than the phase difference that can be resolved by signal processing (Wang, 2016).

Finally, the constructed template-independent measurement model can be simplified and expressed as follows, which denotes the estimation error of TOA attributed to the velocity error.

$$\Delta TOA_2 \approx \frac{1}{cT_{obs}} \mathbf{n} \cdot \left(\int_{t_0}^T \Phi_{rv}(\tau, t_0) d\tau \right) \delta \mathbf{v}(t_0) \tag{19}$$

3. Template-independent navigation method

According to Equation (19), measurements with respect to the velocity error of the vehicle can be obtained without using the pulsar template. However, navigation is not available with access to these measurements of velocity alone, the system is unobservable, the position information of vehicle cannot be calculated.

Extending Equation (11), the state error of the vehicle at an arbitrary epoch t can be predicted by propagating the initial state error by using the orbital transition matrix (Liu, 1992).

$$\begin{cases} \delta \mathbf{r}(t) = \Phi_{rr}(t, t_0) \delta \mathbf{r}(t_0) + \Phi_{rv}(t, t_0) \delta \mathbf{v}(t_0) \\ \delta \mathbf{v}(t) = \Phi_{vr}(t, t_0) \delta \mathbf{r}(t_0) + \Phi_{vv}(t, t_0) \delta \mathbf{v}(t_0) \end{cases} \tag{20}$$

where $\Phi_{vr}(t, t_0)$ and $\Phi_{vv}(t, t_0)$ are the other two partition matrices of the orbital transition matrix.

As shown in Equation (21), in order to achieve system observability, the initial state errors of vehicle can be completely transformed into velocity errors at arbitrary epochs by performing multi-segment observations.

$$\begin{cases} \delta \mathbf{v}_1 = \Phi_{vr}(T_1, t_0) \delta \mathbf{r}_0 + \Phi_{vv}(T_1, t_0) \delta \mathbf{v}_0 \\ \delta \mathbf{v}_2 = \Phi_{vr}(T_2, t_0) \delta \mathbf{r}_0 + \Phi_{vv}(T_2, t_0) \delta \mathbf{v}_0 \\ \dots \dots \dots \\ \delta \mathbf{v}_j = \Phi_{vr}(T_j, t_0) \delta \mathbf{r}_0 + \Phi_{vv}(T_j, t_0) \delta \mathbf{v}_0 \end{cases} \tag{21}$$

where $T_j, j = 1, 2, \dots, n$ represent the end moments of multi-segment observations.

Then we can establish the navigation equations with the term of

$$\begin{cases} \Delta \phi_1 = \frac{f_s}{c(T_1 - t_0)} \mathbf{n} \cdot \left(\int_{t_0}^{T_1} \Phi_{rv}(\tau, t_0) d\tau \right) \delta \mathbf{v}_0 \\ \Delta \phi_2 = \frac{f_s}{c(T_2 - T_1)} \mathbf{n} \cdot \left(\int_{T_1}^{T_2} \Phi_{rv}(\tau, T_1) d\tau \right) \delta \mathbf{v}_1 \\ \dots \dots \dots \\ \Delta \phi_n = \frac{f_s}{c(T_n - T_{n-1})} \mathbf{n} \cdot \left(\int_{T_{n-1}}^{T_n} \Phi_{rv}(\tau, T_{n-1}) d\tau \right) \delta \mathbf{v}_{n-1} \end{cases} \tag{22}$$

To meet the number of state elements, at least six observation segments are required.

Combining Equations (21) and (22), the simultaneous equations can be formed as

$$\Delta \Phi = A \cdot \begin{bmatrix} \delta \mathbf{r}_0 \\ \delta \mathbf{v}_0 \end{bmatrix} \tag{23}$$

where $\Delta \Phi$ expresses the matrix of distort phase differences obtained by dynamic signal processing, A denotes the calculated orbital transition coefficient matrix of the navigation system.

To solve the simultaneous equations, we can build a function optimisation problem, which can be solved easily by the common optimisation algorithms (i.e., genetic algorithm, differential evolution or

particle swarm optimisation) (Kennedy and Eberhart, 1995; Hang and Hang, 2003; Storn and Price, 2006). The strategies of crossover and mutation are improved adaptively to keep diversity of samples and improve the computation efficiency.

In summary, the proposed pulsar-based template-independent navigation method can be complemented by the following procedure (Figure 2):

- 1) Calculate the distort phase difference between the modified observation profile and the directly recovered profile for each data segment by dynamic signal processing.
- 2) Set the elements of δv_0 , δr_0 as variables, substitute them into Equations (21) and (22) to calculate the orbital transition coefficient matrix A with the aid of predicted state information of the vehicle, and then establish the navigation equations.
- 3) Solve the constructed equations, the information of orbit determination or navigation can be achieved directly.

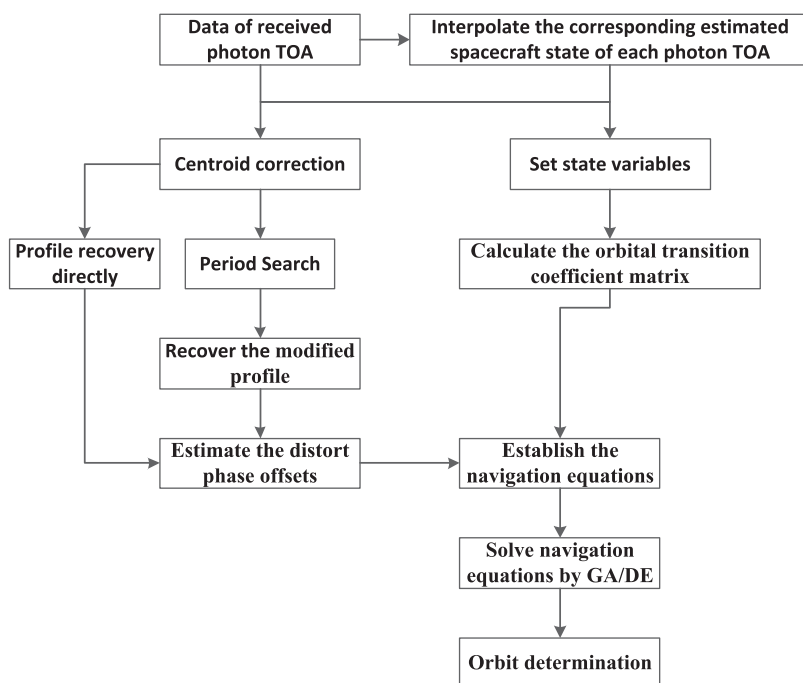


Figure 2. Flow chart of the proposed method.

4. Simulation results

In this section, the simulation data and real data from HXMT and NICER of the Crab pulsar are employed to verify the performance of the proposed method. For simulation data, when the propagation of orbital dynamic is performed, the two-body model is utilised, and the data are generated by adding different initial state errors. For real data, the predicted orbit information used is propagated by adding different initial errors based on the accurate orbit model (Wang, 2016).

4.1. Analysis of theoretical model

4.1.1. Problem of Crab template

In this part, the real data from NICER are utilised to simulate the situation of building the high precision templates in orbit. The phase propagation errors between the templates with different time intervals are analysed.

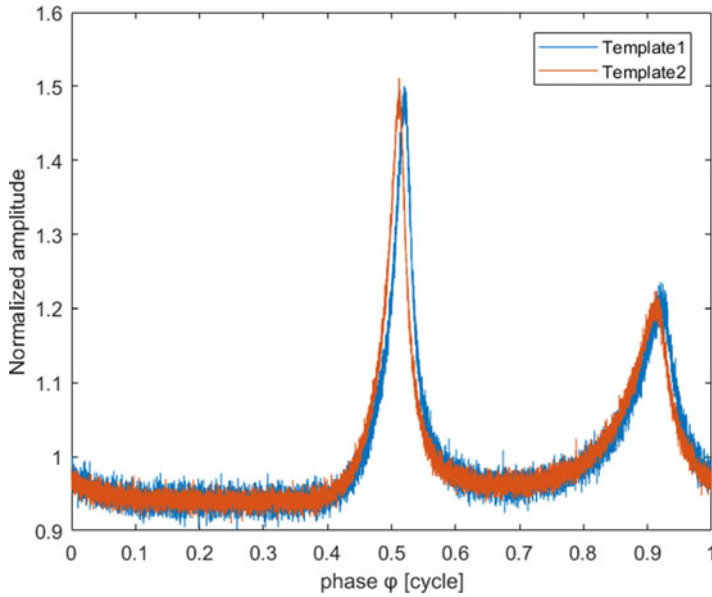


Figure 3. Phase propagation error between the templates with intervals of two months.

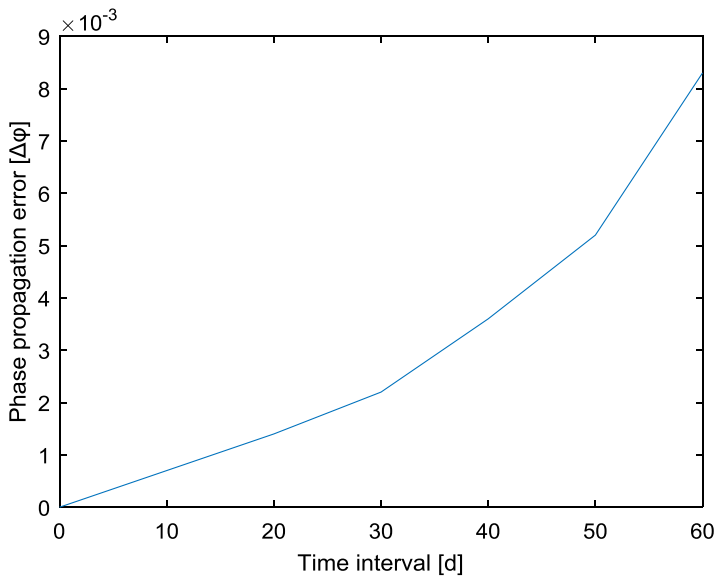


Figure 4. Phase propagation errors between the templates with different intervals.

In Figure 3, the two templates are built separately by the series of photon TOAs detected during September and November 2018. The estimation value of the phase propagation with the time interval is calculated according to the time and phase model, and the first template is translated to the folding moment of the second template. We can see that there exists a certain phase difference between the two templates.

Figure 4 shows the variation of the phase propagation error between the constructed templates with different time intervals. The phase propagation error which may result in an extra position error increases sharply with the time interval. Therefore, it can be concluded that, for the Crab pulsar, the pre-calibrated template cannot be used in the long term and the timing parameters must be updated quite frequently (generally within 10 days).

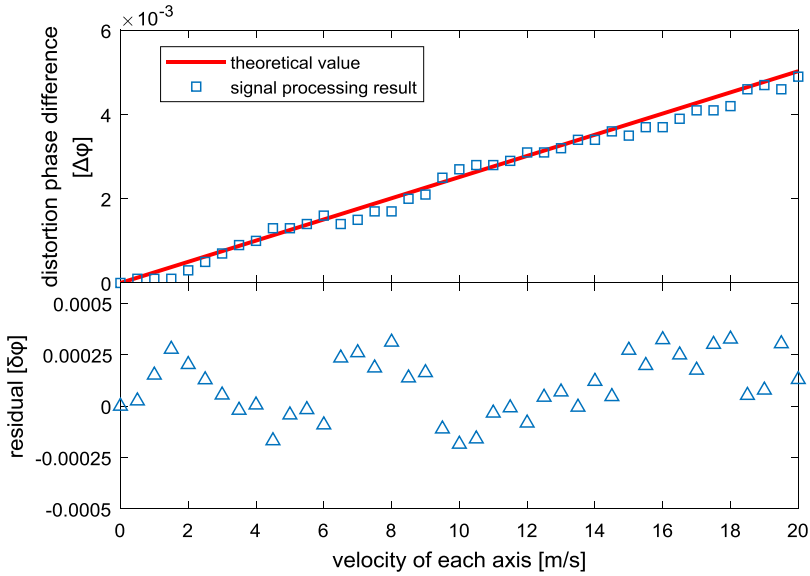


Figure 5. Comparison between the theoretical and the signal processing results with different velocity of vehicle.

Table 1. Simulation parameters of Crab pulsar.

Parameter	Value
α (ph/s)	660
β (ph/s)	13,860.2
Period (ms)	33.4

4.1.2. Feasibility of the derived measurement model

In Section 2, a template-independent measurement model is derived as a term of the velocity error of the vehicle. To verify that the derived model is correct, it is investigated via simulation.

Figure 5 shows the comparison between the signal processing results and the calculation results obtained by the derived theoretical model. The minimum phase resolution of signal processing is 1×10^{-4} . We can see that the set of theoretical results is consistent with the signal processing results. For the comparison result, the mean error is about 1.504×10^{-4} , and the standard variance is about 1.833×10^{-4} .

Therefore, it can be concluded that the measurement model derived in this paper is correct and can be applied to orbit determination or navigation.

4.2. Analysis of the proposed method

4.2.1. Experiments with simulation data

The parameters of the simulated Crab pulsar are listed in Table 1. The pulsar is assumed to be stationary during the observation period and the effect of higher order derivatives of frequency is neglected.

The relationship between the accuracy of distort pulse TOA and the observation time is analysed first, and the result is shown in Figure 6. We can see that the accuracy of the distort pulse TOA increases with observation time, and when the observation time reaches 600–1,000 s, this variation will slow down.

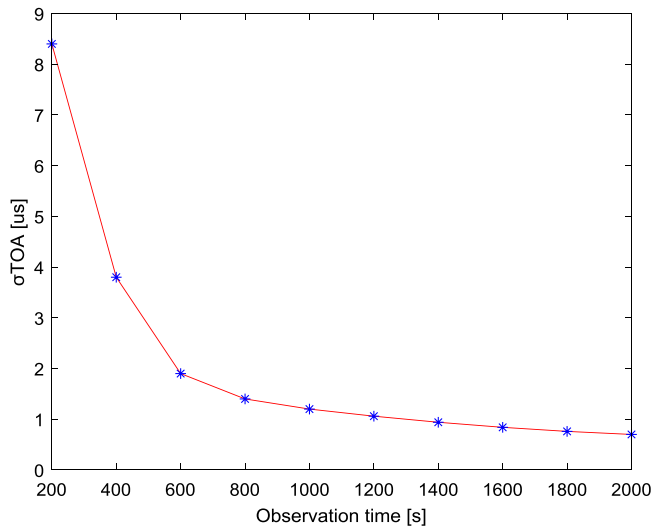


Figure 6. Accuracy of distort pulse TOA in relation to the observation time.

Table 2. Comparison between traditional filtering algorithm and the proposed method.

Item	Position error (km)	Velocity error (m/s)	Calculation time (s)
Proposed method	7.23	7.62	2.32
Filtering algorithm	7.85	6.34	0.95

In this situation, therefore, 20 groups of simulation data were generated with the whole observation period of 6,000 s (each segment about 1,000 s), and the added different initial state errors were randomly produced by uniform distribution.

Figure 7 shows that the navigation result of simulation data, the average estimation error of position and velocity are about 7.23 km and 7.62 m/s. This result demonstrates that the proposed template-independent method is feasible, and can provide the service of orbit determination or navigation with relatively high accuracy.

The superiority of the proposed method over the existing pulsar-based navigation methods is further investigated. Table 2 shows the comparison of navigation performance between the traditional filtering algorithm and the proposed method under the same simulation conditions. It can be seen that the performance of the methods is basically the same. The computational cost of the proposed method is slightly higher but still very low. It should be noted that we can obtain the navigation information directly by this proposed method. For the traditional filtering algorithm, however, it usually takes time to converge the current navigation accuracy.

For the existing pulsar-based navigation methods, pulsar template is the basic input. The phase propagation error existing in the template will directly cause a corresponding extra error in the processing result of the pulse TOA. Considering that the true state of the vehicle cannot be accurately obtained, the template constructed in orbit will also contain a certain phase error. Based on Figure 4, if the template and the timing parameters of the Crab pulsar were not updated in time, the resulting extra position error, which is in proportion, will exceed 10 km. The proposed template-independent method in this paper is not affected by this.

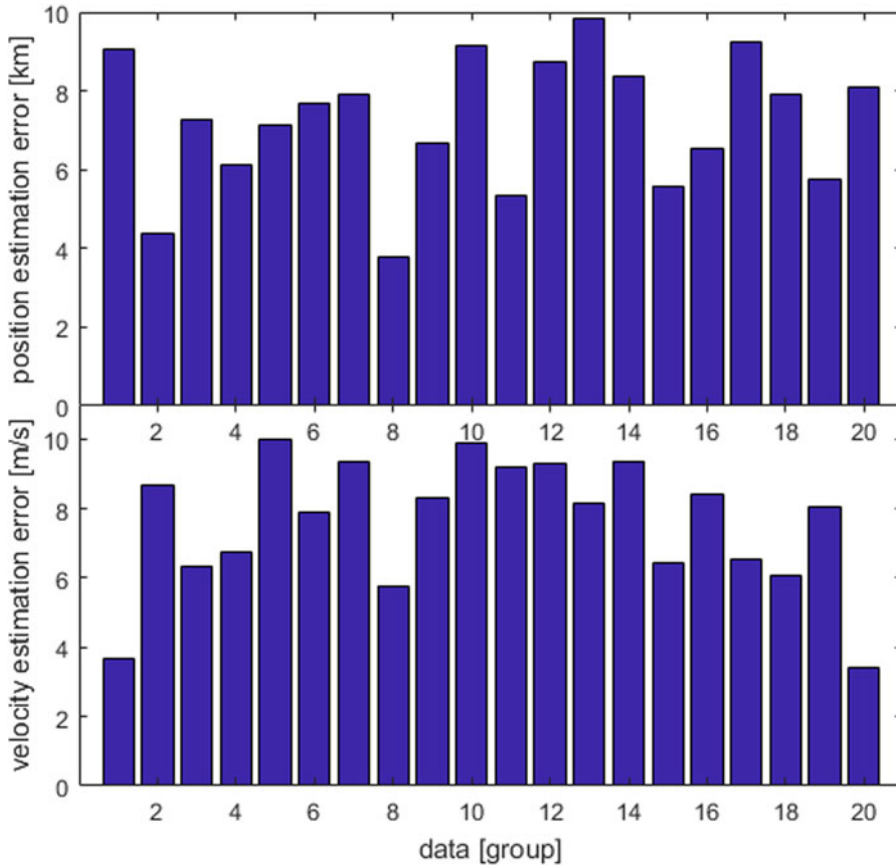


Figure 7. Estimation error of the proposed method for the simulation data.

4.2.2. Experiments with real data

In this part, real data from the Crab pulsar are employed to verify the performance of the proposed method. The initial frequency parameters can be found in the database of Jodrell Bank, UK.

The real observation data from HXMT on 31 December 2018 (Obs_ID: 0101299008) was utilised. Ten groups of data detected by the onboard high energy sensor were chosen with an observation period of more than 3,000 s and Table 3 shows the specifics. Figure 8 shows the navigation results, and the average estimation error of position and velocity are about 9.53 km and 9.89 m/s.

Real observation data from NICER on 26 December 2018 (Obs_ID: 1013010147) were then utilised. Twelve groups of data with observation period more than 2,000 s were chosen and Table 4 shows the specifics.

For the proposed method, it is necessary to divide the chosen data into six segments, which will result in less data per segment. This will have an impact on the navigation performance. Figure 9 shows the navigation results; the average estimation error of position and velocity are about 8.94 km and 9.37 m/s, respectively.

For the real observation data, most groups of the estimation results of position and velocity are better than 10 km and 10 m/s. This also verifies the feasibility of the proposed method. Compared with the navigation results by processing simulation data, the navigation accuracy is lower. This is because, for the model derived in Section 2, the variation of f_s is not considered, which will have an impact on calculating the distort pulse TOA and come to affect the navigation performance. Figure 10 shows the variation of the estimation error of $\Delta\Phi$ by processing simulation and real data. We can see that the phase

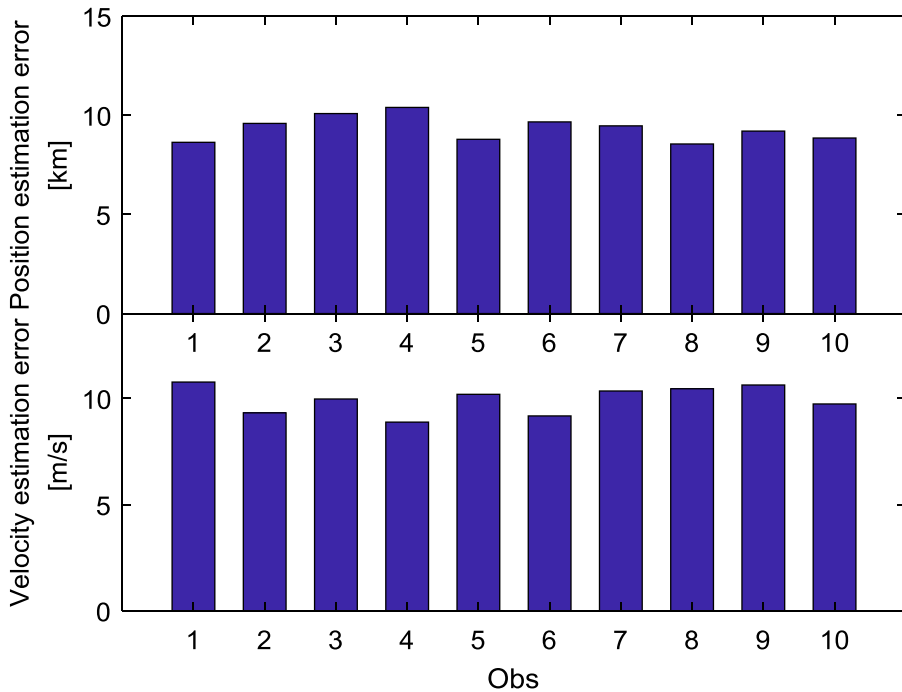


Figure 8. Estimation error of the proposed method for the real data from HXMT.

Table 3. Specifics of real observation data from HXMT.

Obs.	Start and finish time (UTC)	Total time (s)
1	2018-10-31 06:48:29-07:48:17	3588
2	2018-10-31 08:23:55-09:23:42	3587
3	2018-10-31 09:59:20-10:59:07	3587
4	2018-10-31 11:34:45-12:34:33	3588
5	2018-10-31 13:10:11-14:09:58	3587
6	2018-10-31 14:45:36-15:45:23	3587
7	2018-10-31 16:21:02-17:20:49	3587
8	2018-10-31 17:56:27-18:56:14	3587
9	2018-10-31 19:35:57-20:31:40	3343
10	2018-10-31 21:16:58-22:07:05	3007

estimation error increases significantly with time for the real data, and basically remains unchanged for the simulation data.

5. Conclusion

To address the problem that the pre-calibrated template of the Crab pulsar cannot be used in the long term, a simple pulsar-based and template-independent navigation method is proposed in this paper. Different from the existing framework, the correlation between the recovered profiles is derived. Taking the motion of the vehicle into account, the corresponding measurement model is constructed to be a term of the velocity error of the vehicle. Moreover, to achieve the system observability, the state errors can be transformed completely into the velocity errors of the vehicle by performing multi-segment

Table 4. Specifics of real observation data from NICER.

Obs.	Start and finish time (UTC)	Total time (s)
1	2018-12-26 02:06:34-02:41:49	2115
2	2018-12-26 03:39:13-04:14:38	2125
3	2018-12-26 05:11:53-05:47:21	2128
4	2018-12-26 06:44:11-07:20:05	2154
5	2018-12-26 08:16:52-08:52:48	2156
6	2018-12-26 09:49:33-10:25:29	2156
7	2018-12-26 11:22:14-11:58:27	2173
8	2018-12-26 12:54:54-13:30:57	2163
9	2018-12-26 14:27:33-15:03:41	2168
10	2018-12-26 16:00:13-16:36:25	2172
11	2018-12-26 17:32:55-18:09:07	2172
12	2018-12-26 19:05:34-19:41:49	2175

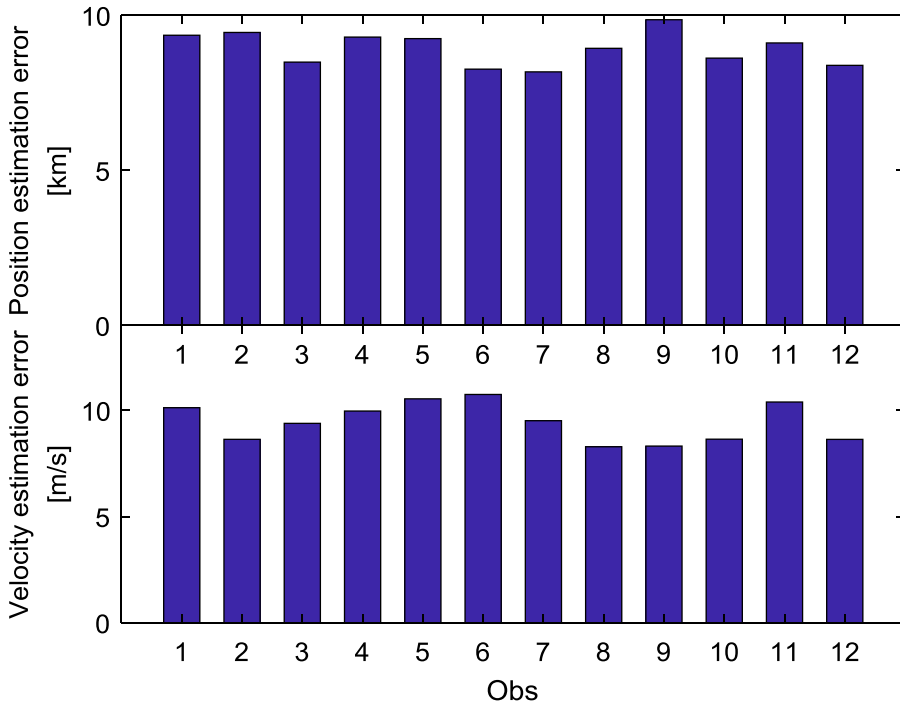


Figure 9. Estimation error of the proposed method for the real data from NICER.

observations. The navigation equations can then be established, and the precise orbit information of the vehicle can be calculated directly. According to the simulation results, the navigation performance is basically consistent with the existing methods based on filtering, and the computational cost is low enough to satisfy the restrictions of an onboard autonomous navigation system.

In summary, the proposed method has the following characteristics. (1) It does not rely on the pulsar template, that is, the performance will not be affected by the template error. The time consumption of building the high precision template can also be saved. (2) It is simple to implement, the navigation information can be obtained directly for each observation. (3) It provides a new idea for pulsar-based navigation and can also extend the application range.

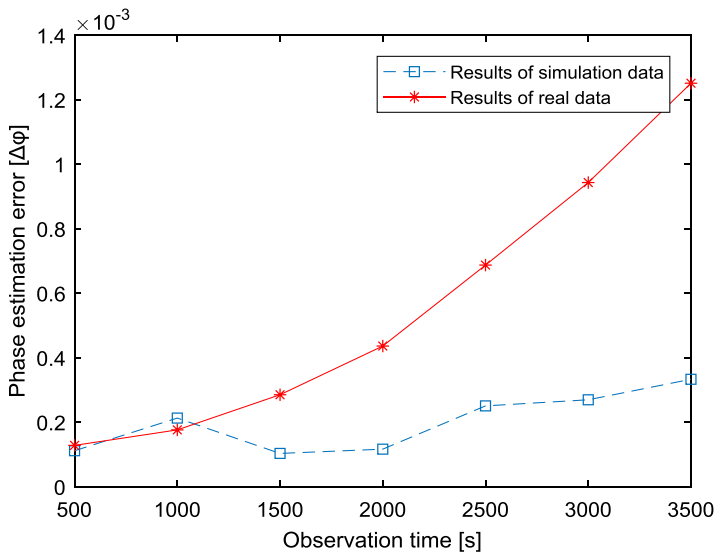


Figure 10. Variation of phase estimation error for using different kinds of data.

References

- Chester, T. J. and Butman, S. A. (1981). *Navigation Using X-Ray Pulsars*. Washington, Pasadena, CA: NASA. Oct. 22–25.
- Emadzadeh, A. A. (2009). *Relative Navigation Between Two Spacecraft Using X-Ray Pulsars*. Los Angeles, CA: University of California.
- Emadzadeh, A. A. and Speyer, J. L. (2011a). *Navigation in Space by X-ray Pulsars*. London: Springer.
- Emadzadeh, A. A. and Speyer, J. L. (2011b). X-ray pulsar-based relative navigation using epoch folding. *IEEE Transactions on Aerospace and Electronic Systems*, **47**, 2317–2328.
- Golshan, R. and Sheikh, S. (2008). *On Pulse Phase Estimation and Tracking of Variable Celestial X-Ray Sources*. San Diego, CA: Institute of Navigation, pp. 101–109.
- Hang, Q. S. and Hang, J. S. (2003). Genetic algorithm for solving ill-conditioned linear system. *Mathematics in Practice and Theory*, **33**, 97–100.
- Hanson, J. E. (1996). *Principles of X-Ray Navigation*. Stanford, CA: Stanford University.
- Huang, L. W., Liang, B. and Zhang, T. (2013). Pulse phase and Doppler frequency estimation of X-ray pulsars under conditions of spacecraft and binary motion and its application in navigation. *Science in China Series G: Physics, Mechanics & Astronomy*, **56**, 848–858.
- Kennedy, J. and Eberhart, R. (1995). Particle Swarm Optimization. *Proceedings of ICNN'95 - International Conference on Neural Networks*, Perth, WA, Australia, 1942–1948.
- Li, F. P. (2015). *Research on Spacecraft Autonomous Navigation Using X-ray Pulsars*. Harbin, China: Harbin Engineering University.
- Li, J. X. and Ke, X. Z. (2011). Maximum-likelihood TOA estimation of X-ray pulsar signals on the basis of Poisson model. *Chinese Astronomy and Astrophysics*, **35**, 19–28.
- Liu, L. (1992). *Artificial Earth Satellite Orbital Dynamics*. Beijing: High Education Press.
- Lyne, A. and Graham-Smith, F. (2005). *Pulsar Astronomy* (3rd ed.). Cambridge, UK: Cambridge University Press.
- Shuai, P., Chen, S. L., Wu, Y. F., Zhang, C. C. and Li, M. (2006). Technology and prospect analysis of X-ray pulsar navigation. *Aerospace*, **10**, 27–32.
- Song, F. N., Zhang, M. J., Zheng, Q. Y., Jin, J. and Pan, X. (2009). X-ray detectors in pulsars-based navigation system. *Journal of Chinese Inertial Technology*, **16**, 682–686.
- Storn, R. and Price, K. (2006). *Differential Evolution—A Simple and Efficient Adaptive Scheme for Global Optimization Over Continuous Space*. Berkeley, CA: University of California.
- Sun, F. H., Bao, M. W., Fang, Y. H. and Li, P. X. (2014). Effect of stability of X-ray pulsar profiles on range measurement accuracy in X-ray pulsar navigation. *Acta Physica Sinica*, **63**, 069701.
- Wang, D. Y. (2016). *X-Ray Pulsar-Based Navigation: Signal Processing and Positioning Algorithms*. Changsha, China: National University of Defense Technology.
- Wang, Y. D. and Zheng, W. (2016a). Pulsar phase and Doppler frequency estimation for XNAV using on-orbit epoch folding. *IEEE Transactions on Aerospace and Electronic Systems*, **2**, 315–333.

Wang, Y. D. and Zheng, W. (2016b). Pulse phase estimation of X-ray pulsar with the aid of spacecraft orbital dynamics. *Journal of Navigation*, **69**, 414–432.

Winternitz, L. M. B., Hassouneh, M. A., Mitchell, J. W., Valdez, J. E., Price, S. R., Semper, S. R., Yu, W. H., Ray, P. S., Wood, K. S., Arzoumanian, Z. and Gendreau, K. C. (2015). X-ray pulsar navigation algorithms and testbed for SEXTANT. *Aerospace Conference*, **4**, 1–14.

Xue, F. M., Peng, L. D., Sun, H. F., Shentu, H., Guo, Y. F., Luo, J. and Chen, Z. K. (2021). X-ray pulsar navigation based on two-stage estimation of Doppler frequency and phase delay. *Aerospace Science and Technology*, **110**, 106470.

Zhang, B. H. (2015). *Theories and Methods of Spacecraft Orbital Mechanics*. Beijing, China: National Defense Industry Press.

Zhang, N. S. (2018a). *The X-Ray Luminosity of the Crab Pulsar Does not Follow its Spin-Down Power During its Largest Glitch Recovery*. Kunming, China: Chinese Astronomical Society.

Zhang, P. D. (2018b). *X-Ray Pulsar-Based Navigation: Data Processing and Verification-Evaluation Technology*. Changsha, China: National University of Defense Technology.

Zhou, Y. Q., Ji, F. J. and Ren, F. H. (2013). Quick search algorithm of X-ray pulsar period based on unevenly spaced timing data. *Acta Physica Sinica*, **62**, 019701.

APPENDIX

Fundamentals of transition matrix in vehicle orbital dynamics

In the Earth-centred or Sun-centred inertial coordinate system, the orbital dynamics model of the vehicle is

$$\begin{bmatrix} \dot{r} \\ \dot{v} \end{bmatrix} = f(x) \tag{A1}$$

where $x = [r^T \ v^T \ a^T]^T$ is the state of the vehicle, and r, v, a are the position, velocity and acceleration of the vehicle.

Linearising the above nonlinear system around the predicted position and velocity, \tilde{r} and \tilde{v} , and obtains

$$\begin{bmatrix} \delta\tilde{r} \\ \delta\tilde{v} \end{bmatrix} = G \begin{bmatrix} \delta r \\ \delta v \end{bmatrix} \tag{A2}$$

where $\delta r(\cdot)$ and $\delta v(\cdot)$ denote the error within the predicted position and velocity and G is the Jacobian matrix and can be expressed as

$$G = \begin{bmatrix} \mathbf{0}_{3 \times 3} & \mathbf{I}_{3 \times 3} \\ S & \mathbf{0}_{3 \times 3} \end{bmatrix} \tag{A3}$$

where

$$S = \left. \frac{\partial \dot{v}}{\partial r} \right|_t \tag{A4}$$

Then, the corresponding discrete linearisation system is

$$\begin{bmatrix} \delta r(t) \\ \delta v(t) \end{bmatrix} = \Phi(t, t_0) \begin{bmatrix} \delta r(t_0) \\ \delta v(t_0) \end{bmatrix} \tag{A5}$$

where $\Phi(t, t_0)$ is the transition matrix with a form of partition matrix as

$$\Phi(t, t_0) = \begin{bmatrix} \Phi_{rr}(t, t_0) & \Phi_{rv}(t, t_0) \\ \Phi_{vr}(t, t_0) & \Phi_{vv}(t, t_0) \end{bmatrix} \tag{A6}$$

An accurate solution of $\Phi(t, t_0)$ can be obtained by solving the following differential equation (Liu, 1992)

$$\begin{cases} \dot{\Phi}(t, t_0) = G\Phi(t, t_0) \\ \Phi(t_0, t_0) = \mathbf{I}_{6 \times 6} \end{cases} \tag{A7}$$

where $I_{6 \times 6}$ is a 6×6 united matrix.

Another way to obtain $\Phi(t, t_0)$ is playing Taylor extensions, i.e.,

$$\Phi(t, t_0) = I_{6 \times 6} + \sum_{m=1}^{\infty} \frac{1}{m!} \Phi^{(m)}(t_0, t_0)(t - t_0)^m \tag{A8}$$

in which $\Phi^{(m)}(t_0, t_0)$ is the m th derivative of $\Phi(t_0, t_0)$.

Although the detailed expression of Equation (A8) is complicated, it can be summarised as a general form of

$$\Phi(t, t_0) = \begin{bmatrix} I_{3 \times 3} + \sum_{m=1}^{\infty} \frac{1}{m!} \varphi_m(t - t_0)^m & \sum_{m=1}^{\infty} \frac{1}{m!} \gamma_m(t - t_0)^m \\ \sum_{m=1}^{\infty} \frac{1}{m!} \theta_m(t - t_0)^m & I_{3 \times 3} + \sum_{m=1}^{\infty} \frac{1}{m!} \varsigma_m(t - t_0)^m \end{bmatrix} \tag{A9}$$

in which $\varphi_m, \gamma_m, \theta_m,$ and ς_m are 3×3 constant matrices and are the m th coefficient matrix of partition matrix in $\Phi(t, t_0)$.

Thus, we have

$$\Phi_{rr}(t, t_0) = I_{3 \times 3} + \sum_{m=1}^{\infty} \frac{1}{m!} \varphi_m(t - t_0)^m \tag{A10}$$

$$\Phi_{rv}(t, t_0) = \sum_{m=1}^{\infty} \frac{1}{m!} \gamma_m(t - t_0)^m \tag{A11}$$

$$\Phi_{vr}(t, t_0) = \sum_{m=1}^{\infty} \frac{1}{m!} \theta_m(t - t_0)^m \tag{A12}$$

$$\Phi_{vv}(t, t_0) = I_{3 \times 3} + \sum_{m=1}^{\infty} \frac{1}{m!} \varsigma_m(t - t_0)^m \tag{A13}$$